Biologically Inspired Navigation Primitives

Iñaki Rañó

Intelligent Systems Research Centre, University of Ulster, Derry, UK Tel.: +44-28-716-75474 Fax.: +44-28-713-75570 i.rano@ulster.ac.uk

Abstract

Because of their apparent simplicity, Braitenberg vehicles have been extensively used in robotics on an empirical basis. However, the lack of a backing up formal theory turns their application into an educated guess of parameter tunning. This paper provides a mathematical model of Braitenberg vehicles 2 and 3 as non-linear dynamical systems, which serves as a theoretical ground to fully exploit them for robotic applications and to create animated agents in artificial life or computer games. The behaviour of the vehicles is analysed using theory of dynamical systems under general conditions, and hints on how to generate desired behaviours are given. Results show that vehicles 2 and 3 can be used to implement bio-inspired navigation like; target reaching and stimulus avoidance, which constitute a set of navigation primitives or basis for navigation behaviour. Through a new theoretical approach, his work paves the way to a proper understanding of Braitenberg vehicles and to an extension of their applicability.

Keywords: Bio-inspired robotics;Local navigation;Dynamical systems modelling and analysis;Braitenberg vehicles

1. Introduction

Braitenberg vehicles [1] qualitatively model sensor based animal steering, and have long been used used on an empirical basis in robotics. The simplest Braitenberg vehicles model the motion of animals towards, or escaping from, a stimulus, known in biology as (positive or negative) taxis behaviour [2]. Animals are very good at moving in the real world and, therefore, they can represent a good model to follow when implementing robotic motion as reflected by the multiple successful empirical applications of Braitenberg vehicles to robotics. While positive taxis is a goal seeking technique, negative

taxis implements avoidance behaviours, both form a basis, or primitives, of navigation behaviour in mobile robots. Because of their simplicity, they are easily understood at an intuitive level without the need of a strong mathematical background, but this is not enough to exploit their full potential. In fact, as a control mechanism for wheeled robots, they are easier to understand by the newcomer to robotics that potential field approach based techniques, and that is why they are sometimes used for teaching [3] [4].

By building up vehicles with sensors wired to their wheels, Braitenberg models complex biological behaviours with great simplicity. Wheels abstract locomotion to focus on steering or guidance level [5], therefore, they can model locomotive configurations like walking, swimming or crawling under standard forward motion conditions. This simplifies the control and analysis of motion, and is a good approximation as forward moving animals, like wheeled vehicles, suffer from non-holonomic restrictions to motion [6]. Braitenberg vehicles can, therefore, be used to design robotic controllers at the steering level. The sensors used by Braitenberg vehicles perceive an abstract stimulus at some point, though the stimulus could also be an artificial potential function. To simulate the omni-directionality of the sensors many empirical applications of Braitenberg vehicles include rings of sensors around the robot.

As shown in figure 1, vehicles 2 and 3 simply consist on direct or crossed connections between the sensors and the motors. Some vehicles have increasing connections such that a stronger stimulus in the sensor generates a faster turn of the associated wheel, while others have a decreasing connection. These vehicles are immersed in environments with a unique kind of stimulus they can perceive. This simplifies the analysis and design of their behaviour while serves as building blocks for more complex vehicles. The combination of direct, crossed, increasing and decreasing connections between the sensors and the wheels of the vehicles generates four different vehicles as presented in figure 1. When sensors on one side are connected to the motors on the same side (ipsilateral) we will talk about a-type or parallel vehicles, while b-type vehicles display a crossed (contralateral) connection as depicted in figures 1(b) and 1(d). Vehicles 2 have an increasing or excitatory connection linking perception to action, represented by the '+' sign on figures 1(a) and 1(b), while for vehicles 3 the connection is decreasing or inhibitory [7].

The behaviour of each vehicle can be qualitatively analysed assuming that a stimulus source in the environment generates a distance decreasing scalar field. Basically, intuition dictates that vehicles 2b and 3a will move towards

high values of the stimulus, and vehicles 2a and 3b will head towards lower values, but sometimes intuition fails in explaining their behaviour [8]. While vehicles 2 might move faster next to the stimulus source, vehicles 3 will slow down as they get close to high stimulus intensity because of the decreasing connection. All these vehicles intuitively generate gradient descent or hill climbing trajectories, while accounting for the non-holonomic constrains to their motion. The simplicity of the control mechanism makes it biologically plausible, while at the same time it is argued [1] that they can produce quite complex behaviours depending on the specific stimulus and internal wiring between sensors and motors.

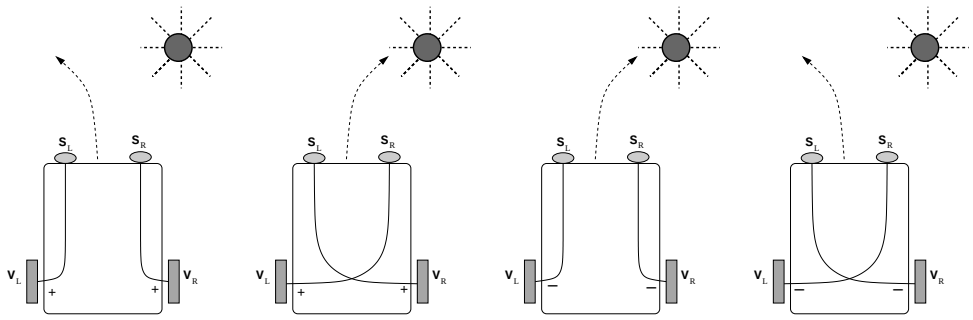

(a) Vehicle 2a (b) Vehicle 2b (c) Vehicle 3a (d) Vehicle 3b

Figure 1: Schematics of Braitenberg Vehicles 2 and 3

As we will see, multiple empirical applications of Braitenberg vehicles can be found in the literature; target seeking, wandering, sound, light or gas source localisation and obstacle avoidance. This paper contributes to the general knowledge of Braitenberg vehicles by delivering a join mathematical model of the control mechanisms of vehicles 2 and 3, and therefore providing theoretical support for these empirical works. Although some behaviour analysis of vehicles 2b and 3a has been presented elsewhere, this paper provides a more exhaustive analysis of all the possible stability conditions, while it also includes vehicles 2a and 3b, not considered in previous works. Moreover, based on this model, new applications can be found [9] [10] for sensor driven robot steering. We use dynamical systems theory to analyse their behaviour, show new theoretical results of their motion and derive design principles to obtain a desired behaviour. Simulations are presented to illustrate the theoretical results.

The paper is organised as follows. The rest of this section presents some robotics applications of Braitenberg vehicles that can be found in the literature. Section 2 states the working assumptions, presents the corresponding mathematical models of the controllers and proposes an analysis that justifies our empirical understanding of Braitenberg vehicles. Section 3 derives general properties of the behaviour of the vehicles, and states additional assumptions that help designing effective controllers for Braitenberg vehicles. The simulations to illustrate the properties of the vehicle trajectories are presented in Section 4. To conclude the paper, a summary of the results, their implications and further working lines are presented in Section 5.

1.1. Related works

Different Braitenberg vehicles have been successfully used on an experimental basis to provide mobile robots with several abilities. However, the lack of a theoretical understanding of this bio-inspired controllers limited their potential applications. Vehicles 3a and 3b for odour source localisation are analysed from an experimental point of view in [11], where the connection between sensors and motors is linear but sensor readings are normalised and averaged. Due to the nature of the stimulus and sensing hardware, a necessary sensor preprocessing introduces a dynamic component in the connection. This is the first application of Braitenberg vehicles to chemical source localisation, a highly complex problem since the stimulus changes with the robot motion. Phonotaxis in a robotic rat is presented in [12] through a model of the peripheral auditory system in mammals. The main contributions of this work are the simplification of sound source localisation through the pinnae and the cochlea model, and a successfully implementation of a model of the central auditive system, with a Braitenberg vehicle 3a to control the robot motion. Another example of phonotaxis behaviour is presented in [13], where the auditory system of a lizard is implemented. In fact, their model of the lizard ear is good enough to work with a high success rate over a wide range of frequencies using a Braitenberg vehicle 2b and a bang-bang controller. Interestingly, the performance of both controllers was similar even though they did not have a model of the vehicle to tune the behaviour of the robot. In a series of works [14] [15] [16] a female cricket phonotaxis model is implemented using spiking neural networks connected according to the excitatory and inhibitory principles of Braitenberg vehicles. This neural model of motion control is comparable to a combination of vehicles 2a and 3b, since excitatory units display a parallel connection between sensors and motors,

while inhibitory ones are crossed. The authors prove their robots perform very well even under quite adverse outdoor conditions. The first robotic implementation of rheotaxis is presented in [10], where a fish robot provided with pressure sensors can keep its orientation relative to a laminar flow. Even though the forward speed is kept fixed, the turning rate of the fish is computed following the principles of Braitenberg vehicles. This is not the only application of these vehicles to underwater robotics, since a robotic electric fish using a similar approach is presented in [17]. In this case the steering control is performed using the difference between the currents, perceived through electrodes, on the sides of the robot. The resulting trajectories approach conductive objects in a pond while avoiding isolating ones. As we can see, Braitenberg vehicles are widely used to implement bio-inspired robotics behaviours, specially when the motion relies on unconventional sensors in the sense that they do not directly provide distance related readings. However, Braitenberg vehicles are also used with proximity sensors in robotics, like sonar, laser and infrared sensors.

The work in [18] implements target acquisition using vehicle 3a, to perform phototaxis, in a combination with vehicle 2b to avoid obstacles using a ring of infrared sensors to simulate omni-directionality. Inspired by this work, [19] presents a wandering mechanism based on a combination of vehicle 2b with stimuli built up from laser and sonar proximity sensors. The stimulus to implement vehicle 2b is a weighted integration of the free area in front of the robot, and, the resulting trajectory is very smooth (at least C^1, since it relies on the integral of a piece-wise continuous function, the distance to the obstacles). Through infra-red based fuzzy controllers that generate offset velocities on each wheel, Braitenberg vehicles 3a and 2b are used for local navigation in [20]. Goal seeking is implemented by vehicle 2b while vehicles 3b and 2a are used to avoid obstacles in the front and back of the robot respectively. A Lego vehicle with a hardware implementation of the vehicle 3b for obstacle avoidance and a wall following behaviour is presented in [21]. The power supply of the wheels is connected in a decreasing way to infrared sensors placed in the front of the robot, which makes the vehicle to slow down when objects are detected.

2. Assumptions and Models of Vehicles 2 and 3.

Like in the original work of Braitenberg we will assume the environment consists on a single stimulus the vehicle can measure through its sensors.

This stimulus can be modelled as a non-negative two dimensional smooth function of the position, $S(\mathbf{x}) \in C^2$ for $\mathbf{x} \in D \subset \Re^2$, where the workspace D is a simply connected subset of $\Re^2$. These stimuli can be a light source (following the inverse-square law $S(\mathbf{x}) \propto 1/r^2$), a sound source ($S(\mathbf{x}) \propto 1/r$), the free area around a robot or any artificial potential, as we saw in the previous section. The relation between the perceived stimulus and the velocity of the wheels can be modelled as a C^2 function $F(s)$ taking non negative values. This function is increasing for vehicles 2 and decreasing for vehicles 3, which actually implies it has, respectively, positive or negative derivative on its domain, i.e. $F'(s) > 0$ for vehicle 2 and $F'(s) < 0$ for vehicle 3. Therefore, we can write $v_{r/l} = F(s)$ where 's' is the stimulus value on the sensor and '$v_{r/l}$' is the speed of the wheel. The restriction on the image of $F(s)$ being $\Re^+ \cup \{0\}$ forbids the vehicle to move backward but allows it to stop completely, generally, a biologically plausible assumption.

2.1. The Controller of Braitenberg Vehicles

Given the above assumptions we can now derive a mathematical expression for the controller. Figure 2 shows the configuration of the sensors in the front of the vehicle. We will denote $\mathbf{x}$ the midpoint and δ the distance between the sensors. Since the vehicle has a heading direction θ, we can define a unit vector linked to the front of the vehicle $\hat{e}^T = [\cos\theta, \sin\theta]$ pointing in the direction of the vehicles' motion and $\hat{e}_p^T = [-\sin\theta, \cos\theta]$, a vector orthogonal to $\hat{e}$, pointing to the left side of the vehicle. Approximating the function composition $F(S(\mathbf{x}))$ as a Taylor series around the mid point between the sensors and transforming wheel velocities into global velocities (see appendix A), we obtain:

$$v \approx F(S(\mathbf{x})) + \frac{\delta^2}{4}\hat{e}_p^T D^2 F(S(\mathbf{x}))\hat{e}_p \quad (1)$$

$$\omega \approx \mp\frac{\delta}{d}\nabla F(S(\mathbf{x}))\hat{e}_p \quad (2)$$

where d is the wheelbase, $\nabla F(S(\mathbf{x})) = \frac{dF}{dS}\nabla S(\mathbf{x})$ is the gradient of the composite function, $D^2F(S(\mathbf{x})) = \frac{d^2F}{dS^2}\nabla S(\mathbf{x})\nabla^T S(\mathbf{x}) + \frac{dF}{dS}D^2S(\mathbf{x})$ is the Hessian matrix, and the different signs on equation (2) correspond to a-type or parallel (minus) and b-type or crossed (plus) vehicles. These equations are the result of truncating the Taylor series of the wheel velocities on the second

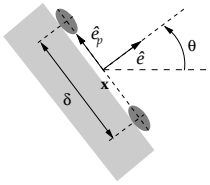

Figure 2: Coordinate system at the Front of the vehicle

order terms, and provide a way of analytically deal with Braitenberg vehicles or to run accurate simulations of their behaviour.

2.2. Intuitive analysis of the controller

Equation (1) shows that the first order approximation of the linear velocity of the vehicle depends on the stimulus at the midpoint between the sensors, specifically, the forward velocity is just $F(s)$. Therefore, to control the linear velocity, the two sensors can be substituted by one at the centre of the vehicle. This matches our intuition on how the vehicles behave, as high values of the stimulus $S(\mathbf{x})$ generate high speeds for vehicles 2 and low ones for vehicles 3. It is worth noting that the velocity equation is independent on the type of vehicle, but the properties of $F(s)$ are very different for each vehicle ('2' and '3'). The error on the approximation, the difference between the real and modelled speeds, depends on second order terms, i.e. on the Hessian of $F(S(\mathbf{x}))$ and the distance between the sensors.

The approximation for the angular velocity ω shows that the turning rate depends on the directional derivative of the stimulus along the direction of the sensors, orthogonal to the vehicle heading. Equation (2) can be written as $\omega = \mp\frac{\delta}{d}\partial_{\hat{e}_p}F(S(\mathbf{x}))$, where $\partial_{\hat{e}_p}$ represents the directional derivative of $F(S(\mathbf{x}))$ along $\hat{e}_p$. The angular velocity is multiplied by the morphological scaling factor $\frac{\delta}{d}$. This is the result of sampling the stimulus at two different points, and, similarly to the linear speed, the turning rate can be understood as a gradient measuring sensor, located at the midpoint between the vehicle's sensors.

Assuming the vehicle cannot move forward, the gradient at one point $\mathbf{x}_0$ will be a constant vector we can write as $F'(S(\mathbf{x}_0))||\nabla S(\mathbf{x}_0)||\hat{e}_{\theta_0}$, where the sign of $F'(S(\mathbf{x}_0))$ is different for vehicles '2' and '3', $||\nabla S(\mathbf{x}_0)||$ is the module of the gradient at $\mathbf{x}_0$ and $\hat{e}_{\theta_0} = [\cos\theta_0, \sin\theta_0]^T$ is a unit vector along the direction of the gradient. Since $\omega = \dot{\theta}$, we can rewrite the angular velocity

equation for the static vehicle as:

$$\dot{\theta} = \mp\frac{\delta}{d}F'(S(\mathbf{x}_0))||\nabla S(\mathbf{x}_0)||\sin(\theta_0 - \theta) \quad (3)$$

Equation (3) represents an autonomous dynamical system in the heading direction with two equilibrium points, $\theta = \theta_0$ and $\theta = \theta_0 + \pi$, which correspond to the vehicle heading the gradient and its opposite direction. One equilibrium point will be stable and one unstable, though to identify the stable one we need to consider the sign of $F'(s)$. It can be seen that the vehicle 2a, with $F'(s) > 0$, and the vehicle 3b, with $F'(s) < 0$ on equation (2) align their heading with the gradient, i.e. the stable equilibrium point is θ_0. The other two vehicles perform a gradient descent on the stimulus such that the stable equilibrium point is $\theta = \theta_0 + \pi$. It is worth noting that the slope of $F(s)$ has a direct impact on the reaction time of the angular controller, and therefore to make the vehicle turn faster for a given stimulus we need a steeper $F(s)$ function. This provides a design criterion for Braitenberg vehicles, that is, the slope of $F(s)$ controls the reaction or relaxation time of the heading of the vehicle when converging to the gradient direction. On the other hand, the turning rate is also controlled by the projection of the gradient of $S(\mathbf{x})$ along the direction of the vehicle, such that the turning rate is maximal when the vehicle direction is orthogonal to the gradient.

The performed analysis is also valid for any general C^1 stimulus and $F(s)$ function, and clearly, the smaller the distance between the sensors the more accurate the approach will be. Even though this analysis formally explains our intuition on how Braitenberg vehicles work, a deeper analysis is needed to understand their real behaviour.

3. General Analysis of the vehicles' behaviour

To analyse the trajectories of the vehicles we will substitute the approximated controller, equations (1) and (2), in the unicycle model – a kinematic, under-actuated non-linear motion model – to obtain:

$$\dot{x} = F(S(\mathbf{x}))\cos\theta \quad (4)$$

$$\dot{y} = F(S(\mathbf{x}))\sin\theta \quad (5)$$

$$\dot{\theta} = \mp\frac{\delta}{d}\nabla F(S(\mathbf{x}))\cdot\hat{e}_p \quad (6)$$

where $\mathbf{x} = [x, y]^T$ and the state space of the dynamical system describing the behaviour is $D \times \mathcal{S}^1$. Even though these equations model simultaneously vehicles 2 and 3, each case has to be analysed separately since the shape of $F(S(\mathbf{x}))$ depends on the vehicle.

Before performing the analysis, we will assume the value of the stimulus falls in the range $[s_0, s_1]$, i.e. $s_0 \leq S(\mathbf{x}) \leq s_1$ for all $\mathbf{x} \in D$, such that $S(\mathbf{x}) = s_0 \iff \mathbf{x} \in \partial D$, the lowest value appears at the workspace boundary. This provides a design criterion for the stimulus function if it has to be built, for instance, as an artificial potential. So far we assumed $F(s)$ is non-negative but we will impose the additional constraint $F(s_0) = 0$ for vehicles 2, and $F(s_1) = 0$ for vehicles 3, while the function value at the other end is bounded. These conditions allow having equilibrium points in the corresponding dynamical system, otherwise equations (4) and (5) would never become zero simultaneously. In fact, these should be design conditions for applications of Braitenberg vehicles in robotics.

A common technique to analyse the stability of an equilibrium point of a dynamical system is the linear stability test, i.e. analysing the eigenvalues of the Jacobian matrix. In our case the Jacobian matrix can be stated as:

$$J = \begin{bmatrix} \hat{e}\nabla F(S(\mathbf{x}))^T & F(S(\mathbf{x}))\hat{e}_p \\ \mp\frac{\delta}{d}\nabla F_{x|y}(S(\mathbf{x}))^T\hat{e}_p & \pm\frac{\delta}{d}\partial_{\hat{e}}F(S(\mathbf{x})) \end{bmatrix} \tag{7}$$

where $\nabla F_{x|y}(S(\mathbf{x}))^T\hat{e}_p$ is a row sub-matrix containing the partial derivatives of the gradient w.r.t. x and y, and $\partial_{\hat{e}}F(S(\mathbf{x}))$ is the directional derivative of $F(S(\mathbf{x}))$ along $\hat{e} = [\cos\theta, \sin\theta]^T$. The equilibrium points of the system will be stable if all the eigenvalues of the Jacobian are negative or have negative real parts, and unstable otherwise. Another way of using the Jacobian to assess stability, is to evaluate it along a known solution trajectory of the system to test whether neighbouring trajectories get closer to, or diverge from, it. This is the generalisation of the linear stability test for non equilibrium trajectories of the dynamical system, and is represented in figure 3, where the trajectory $\mathbf{x}(t) + \Delta\mathbf{x}(t)$, close to $\mathbf{x}(t)$, diverges from it. In this case, the evaluation of the Jacobian should be performed along the points $\mathbf{x}(t)$, $\theta(t)$.

3.1. Vehicles 2

Under the assumption that the stimulus takes its minimum value at the boundary ∂D, it can be proved that the trajectories of the vehicles 2 are

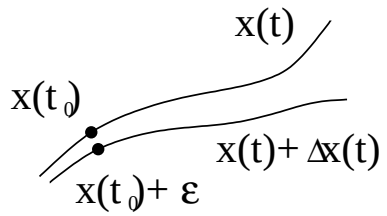

Figure 3: Evolution of two close trajectories

actually restricted to D. This is the consequence of the flow defined by the dynamical system (4), (5) and (6), having no component pointing out the surface $\partial D \times \mathcal{S}^1$. Since $F(S(\mathbf{x})) = 0$ for $\mathbf{x} \in \partial D$, the first two components of the vector field vanish at the boundary. The third component will only vanish for angles θ orthogonal to the gradient. However, the normal vectors to the surface $\partial D \times \mathcal{S}^1$ have no angular component, and therefore, the dot product of the surface normal and the flow defining the vehicle motion is zero, either because they are orthogonal to each other or because the flow completely vanishes. This means no flow comes out of the state space and, therefore, vehicle 2 motion will be bounded in the workspace by the contour ∂D. From a design viewpoint, we can restrict the motion of a Braitenberg vehicle on a stimulus field $S(\mathbf{x})$ by selecting a level curve with a value s_0 and a controller function $F(s)$ such that $F(s_0) = 0$, which justifies our previous assumptions. On the other hand, if the motion of the vehicle has to be restricted by a closed curve Γ, we need to design $S(x)$ such that Γ is a level-set of $S(x)$. These design criteria have not been explicitly identify before, are derived from our theoretical model, and have been exploited in [9] to implement a bounded wandering behaviour in a real robot which densely covers the free space without colliding with obstacles.

Since $F(S(\mathbf{x})) \neq 0 \forall \mathbf{x} \in D$, the only equilibrium points of vehicles 2a and 2b lay in the workspace boundary ∂D. If the gradient of $S(\mathbf{x})$ vanishes at some points of ∂D, these points will belong to the set of equilibrium points. If the gradient does not vanish at ∂S, the equilibrium points can be obtained by solving $\nabla S(\mathbf{x})^T \hat{e}_p = 0$ for any $\mathbf{x} \in \partial D$, which gives at least two solutions for θ, since for each point $\mathbf{x} \in \partial D$ we can find two complementary angular values which make $\dot{\theta} = 0$. These points are such that the vehicle heads in the direction of the gradient $\nabla S(\mathbf{x})$ or in the opposite direction. Now we will analyse separately, using the linear stability test, the behaviour of

Braitenberg vehicles 2 in the boundary ∂D and inside the workspace.

3.1.1. Behaviour at the Boundary points

Equilibrium points exist at the boundary and the linear stability test can be used to test their stability. In the case of the gradient vanishing in ∂D, if we substitute $F(S(\mathbf{x})) = 0$ and $\nabla S(\mathbf{x}) = \mathbf{0}$ in (7) we obtain only zero eigenvalues and, therefore, the linear test gives no information about the stability of the equilibria at $\partial D \times \mathcal{S}^1$. More sophisticated methods, as presented for the two dimensional case in [22], need to be applied. However, if the gradient of the stimulus is not zero at the boundary, the eigenvalues of the Jacobian matrix can be computed to evaluate the stability of the equilibrium points. Disregarding the effect of the zero eigenvalue, which corresponds to the direction of motion restricted by the non-holonomic condition, for the vehicle 2a the other two eigenvalues are $\lambda_{2a} = \left\{\pm||\nabla F(S(\mathbf{x}_0))||, \pm\frac{\delta}{d}||\nabla F(S(\mathbf{x}_0))||\right\}$ and for vehicle 2b $\lambda_{2b} = \left\{\pm||\nabla F(S(\mathbf{x}_0))||, \mp\frac{\delta}{d}||\nabla F(S(\mathbf{x}_0))||\right\}$. The sign of the eigenvalues depends on the heading of the vehicle relative to the gradient.

On the one hand, for vehicle 2a, the sign of the two eigenvalues is the same for a given heading solution of $\nabla S(\mathbf{x})^T \hat{e}_p = 0$. This means that one of the solutions will be stable and the other unstable. Specifically, the stable equilibrium point corresponds to the vehicle heading the opposite direction of the gradient, and the unstable equilibrium to the vehicle heading the gradient. Therefore, the dimension of the, respectively, stable and unstable manifolds for these points is two, while the third dimension corresponds to a central manifold (the zero eigenvalue). Since for each point in ∂D there is a stable equilibrium point, with a two dimensional basins of attraction, this effectively covers the whole state space. This means vehicle 2a will approach the boundary ∂D if it points towards it, and will escape for headings pointing in the opposite direction. However, as the stable manifolds of the equilibrium points cover the whole workspace, the vehicle will always approach one of these stable equilibrium points on the boundary. Eventually, vehicle 2a will always reach the boundary of the stimulus and will stay there as stable equilibria exist. This result matches our intuitive understanding of how the vehicle works, and makes Braitenberg vehicle 2a suitable to avoid high values of a stimulus or potential function.

On the other hand, for vehicle 2b, the equilibrium points always have eigenvalues with opposite signs and therefore all existing equilibria on the state space corresponding to $\mathbf{x} \in \partial D$ are unstable. Contrary to the 2a case, all the equilibrium points have a 1D stable manifold. This means that a

direction exists such that the equilibrium point can be reached, when the vehicle heads exactly the opposite direction of the gradient. However, they form a zero measurement set of the state space and any small perturbation will drive the vehicle away from this point. In the case of a stimulus source this situation corresponds to the vehicle having the source exactly on its back. There is no way (but from the stable manifold) the vehicle 2b will reach the boundary ∂D and it will wander around D as there is no other equilibrium point. As we saw in the related works, Braitenberg vehicle 2b can therefore be used to implement wandering behaviour in a bounded workspace [9].

3.1.2. Behaviour in the open set

To apply the linear stability test in the interior points we need to obtain a solution trajectory and compute the Jacobian matrix along it. The eigenvalues along time will determine how nearby trajectories behave.

If we assume the gradient of $S(\mathbf{x})$ has locally a constant direction and the vehicle's orientation coincides with the direction of the gradient of $S(\mathbf{x})$, the directional derivative along $\hat{e}$ appearing in the expression (7) corresponds to the signed length of the gradient. Under these conditions the vehicle will locally follow a straight line trajectory as the directional derivative along $\hat{e}_p$ will be zero. The Jacobian can be simplified and its eigenvalues that can be computed as:

$$\lambda_1 = \partial_{\hat{e}} F(\mathbf{x}) \tag{8}$$

$$\lambda_2 = \pm\frac{\delta}{2d}\partial_{\hat{e}} F(\mathbf{x}) \left[1 + \sqrt{1 \mp 4\frac{d}{\delta}\frac{\kappa F(\mathbf{x})}{|\partial_{\hat{e}} F(\mathbf{x})|}}\right] \tag{9}$$

$$\lambda_3 = \pm\frac{\delta}{2d}\partial_{\hat{e}} F(\mathbf{x}) \left[1 - \sqrt{1 \mp 4\frac{d}{\delta}\frac{\kappa F(\mathbf{x})}{|\partial_{\hat{e}} F(\mathbf{x})|}}\right] \tag{10}$$

where $F(\mathbf{x}) = F(S(\mathbf{x}))$, the directional derivative $\partial_{\hat{e}} F(\mathbf{x})$ is the signed norm of the gradient and $\kappa = \frac{\hat{e}_p^T HF(\mathbf{x})\hat{e}_p}{|\partial_{\hat{e}} F(\mathbf{x})|}$, is the curvature of the contour line of $S(\mathbf{x})$ at the position of the vehicle, with $HF(\mathbf{x})$ being the Hessian matrix of $F(\mathbf{x})$. The positive sign of λ_2 and λ_3 corresponds to a-type or parallel vehicle and the negative to crossed or b-type. Since the local behaviour of the vehicle relative to a straight line trajectory depends on the curvature of the contour lines, we need to analyse the eigenvalues for possible values of κ.

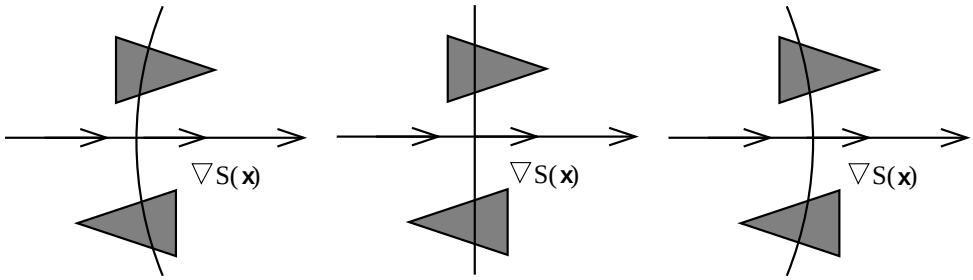

(a) Negative curvature (b) Zero curvature (c) Positive curvature

Figure 4: Possible configurations of the vehicle aligned with a stimulus gradient

We can use the linear stability test evaluating the above eigenvalues along the linear trajectory and check whether close trajectories converge or diverge locally. First, the eigenvalue λ_1 is the directional derivative of $F(S(\mathbf{x}))$ along the heading direction, which, since $F'(s) > 0$ for vehicles 2, is positive if the vehicle heads the gradient and negative if it heads the opposite direction. Therefore, there will always be a unstable one dimensional manifold if the vehicle heads in the direction of the gradient and a stable one for the opposite direction.

The other two eigenvalues (λ_2 and λ_3) depend on the type of vehicle (a or b), on the curvature κ, on the linear velocity of the vehicle and the length of the gradient. The possible configurations of the vehicle and κ are presented in figure 4. On the one hand, for a-type vehicles and $\kappa = 0$, the set up presented in figure 4(b), λ_2 has the same sign as λ_1, while the third eigenvalue becomes zero. Therefore, for a planar stimulus all the eigenvalues will have the same sign and vehicle 2a will always head in the opposite direction of the gradient, i.e. it will move towards decreasing stimulus values. This is the expected outcome of Braitenberg vehicle 2a, since it intuitively moves towards low values of the stimulus. On the other hand, since the two eigenvalues (at least one of them) for vehicle 2b have opposite sign to λ_1 there will always exist an unstable manifold for both directions in the case of $\kappa = 0$. This is consistent with the resulting behaviour at the boundary for vehicles 2b.

As the curvature of the contour lines increases in absolute value, the eigenvalues can change to generate different behaviour. The trajectories of vehicle 2a, for instance, can display oscillatory behaviour for $\kappa > 0$ since λ_2 and λ_3 can become complex numbers. When the vehicle heads the gradient

	$\kappa < 0$		$\kappa = 0$		$\kappa > 0$	
	$\partial_{\hat{e}} S > 0$	$\partial_{\hat{e}} S < 0$	$\partial_{\hat{e}} S > 0$	$\partial_{\hat{e}} S < 0$	$\partial_{\hat{e}} S > 0$	$\partial_{\hat{e}} S < 0$
a	UUS	SSU	UUZ	SSZ	UUU	SSS
b	USS	SSU	UZS	SZU	UUS	SSU

Table 1: List of the local stability results of the eigenvalue analysis for vehicles 2a and 2b

direction, the oscillation will not be noticeable because all the eigenvalues have positive real part. If the vehicle is moving towards low stimulus values when all the eigenvalues have negative real part, oscillatory trajectories could be observed locally. As the linear velocity of the vehicle ($F(S(\mathbf{x}))$) decreases the imaginary part of the eigenvalues λ_2 and λ_3 will eventually become zero and oscillations will stop as Braitenberg vehicle 2a approaches the boundary of the workspace. Vehicle 2b, on the other hand, will always show trajectories diverging from the gradient direction for positive κ with no oscillation, since the term inside the square root will always be positive.

When the curvature of the contour line of $S(\mathbf{x})$ is negative the oscillatory behaviour appears for vehicle 2b. However, since linearised equations of vehicle 2b always have at least one unstable manifold, the effect of the oscillations will not be noticeable. In exchange, what can occur is that the vehicle 2a diverges from the gradient descent trajectory if the product of the curvature and the linear velocity is too high. Table 1 summarises the analysis of all the possible situations where 'S' denotes stable trajectories close to the gradient direction, 'U' denotes unstable and 'Z' denotes a zero eigenvalue. It is worth reminding that the stability conditions of the table represent whether the trajectories converge with respect to a vehicle following locally the gradient, or the opposite, direction. The conditions $\partial_{\hat{e}} S > 0$ and $\partial_{\hat{e}} S < 0$ represent the configurations of the vehicle heading the gradient and opposite directions respectively. The table is therefore useful for designing Braitenberg vehicle controllers as it can be, for instance, read as when care must be taken at choosing the linear velocity ($F(s)$) such that the oscillatory behaviour is avoided. It also signals that vehicle 2a has most of the times stable behaviour when heading the gradient descent direction and unstable otherwise, so it is suitable to implement stimulus avoidance behaviours. The opposite occurs for vehicle 2b, since there is always a unstable manifold for any configuration close to the straight line trajectory, which means the trajectory of the vehicle is sensitive to initial conditions, a feature of chaos [23].

3.2. Vehicles 3

According to our assumptions, vehicles 3 will have a non zero forward velocity in D but also in its contour ∂D, therefore they can move outside their workspaces. This occurs, for instance, when the position of the vehicle is close to ∂D and its heading direction $\hat{e}$ is close to the direction of the gradient of $F(S(\mathbf{x}))$. On the other hand, the minimum of the velocities occurs at the interior of the set, since $F(s_1) = 0$, therefore, the only equilibrium points for these vehicles are at the maximum of $S(\mathbf{x})$, and they will stay within D if the equilibrium points are stable and their poses belong to the basin of attraction of such equilibria. If we want the vehicle to reach a specific stimulus value, we ought to select $F(s)$ to vanish at that value, but this is only a necessary condition. On the other hand, if we are free to choose $S(\mathbf{x})$, we would do it such that the potential function will present a maximum at the target point where $F(s)$ vanishes. We will consider only the configuration of vehicles 3 close to the equilibrium points as it provides information of whether the trajectories might be stable or not, i.e. whether a basin of attraction might exist at all.

3.2.1. Behaviour at the maximum

The analysis of vehicles 3 shows that equilibrium points can only appear at the maximum of the stimulus since $F(s_1) = 0$. If the gradient also vanishes, for any heading (any $\hat{e}_p$) the equation (6) will be $\dot{\theta} = 0$. This means that there will be an equilibrium set in the state space, the points where $F(s) = 0$ for any heading of the vehicle. Unless $F(s)$ is designed to vanish for some stimulus value (s_1 in our case) the behaviour of Braitenberg vehicles 3 will have no equilibrium point and it will move around without stopping, which is not a desirable behaviour for target reaching. The linear analysis of the equilibrium point brings no information about the stability if the points where $S(\mathbf{x}) = s_1$ are also maxima of $S(\mathbf{x})$, since the eigenvalues vanish. However, intuitively it should be stable for vehicle 3a and unstable for vehicle 3b. Formal stability tests require more sophisticated techniques in this case [22].

If, instead of an isolated point, the set of $\mathbf{x}$ such that $S(\mathbf{x}) = s_1$ is a level curve but not a maximum of $S(\mathbf{x})$, preferred equilibrium directions will appear as for vehicles 2 in the previous section. These directions correspond to the solutions of $\partial_{\hat{e}_p} F(\mathbf{x}) = 0$ and, therefore, two equilibrium points appear. The linear stability test can be used again in this case for trajectories close to the gradient direction at the equilibrium points or, in general, like in the previous section, trajectories close to a straight line trajectory. The analysis

	$\kappa < 0$		$\kappa = 0$		$\kappa > 0$	
	$\partial_{\hat{e}} S > 0$	$\partial_{\hat{e}} S < 0$	$\partial_{\hat{e}} S > 0$	$\partial_{\hat{e}} S < 0$	$\partial_{\hat{e}} S > 0$	$\partial_{\hat{e}} S < 0$
a	SSU	UUS	SSZ	UUZ	SSS	UUU
b	SUU	USS	SZU	UZS	SSU	UUS

Table 2: List of the local stability results of the eigenvalue analysis for vehicles 3a and 3b

can be performed using the eigenvalues (8), (9) and (10), but in this case $F'(s) < 0$ and, therefore, the eigenvalue λ_1 will be positive for vehicles 3 heading the opposite direction of the gradient of $S(\mathbf{x})$.

Considering the case $\kappa = 0$, the sign of λ_2 and λ_1 are the same for vehicle 3a and, therefore, the gradient ascent direction is stable. The opposite occurs for vehicle 3b, as the eigenvalue λ_2 is positive if λ_1 is negative. The whole analysis of the stability of local trajectories as a function of the curvature of the stimulus isolines and vehicle heading can be performed for vehicles 3, and the resulting stability conditions are presented in table 2. While vehicle 3a shows stable trajectories in the gradient ascent direction, if the vehicle heads the opposite direction of the gradient the trajectories will diverge locally. On the other hand, vehicle 3b has for all cases a unstable manifold, therefore it will display a locally divergent behaviour. Consequently, Braitenberg vehicle 3a can be used for target reaching, while vehicle 3b seems appropriate for avoidance tasks. It is worth noting that vehicle 3a does not always have a stable equilibrium point, and therefore, the sufficient condition for the trajectories to converge to the gradient direction is $\kappa > 0$. If the stimulus around the maximum can be approximated by a parabolic function several straight line trajectories exist for these vehicles that correspond to the principal axes of the parabola. Table 2 also captures the behaviours of trajectories close to the main axis of the stimulus.

4. Simulations

In order to illustrate the behaviour of the Braitenberg vehicles we performed different simulations integrating equations (4), (5) and (6) for different stimuli $S(\mathbf{x})$ and $F(s)$ functions. This section also illustrates how to define stimulus functions of the position, for instance, that can be used to implement controllers for different types of behaviour using Braitenberg vehicles. The amount of possible configurations relative to the gradient direction is high, and therefore, we will illustrate only the general behaviour

i	g_i	α_i	Σ_i	$\mathbf{x}_i^0$
1	10	-0.1	$\begin{bmatrix} 1 & 0.2 \\ 0.7 & 3 \end{bmatrix}$	$[0, 0]$
2	-1	0.8	$\begin{bmatrix} 1 & 0 \\ 0 & 1 \end{bmatrix}$	$[5, -2]$
3	-1	0.6	$\begin{bmatrix} 0.7 & 0.3 \\ 0.2 & 1 \end{bmatrix}$	$[-6, 1]$

Table 3: Parameters for the stimulus function $S(\mathbf{x})$ on the simulation of vehicle 2a

of the vehicles, which can be used to implement navigation primitives like target seeking or avoidance behaviour. On the other hand, since these simulations are based on our analytic expressions for Braitenberg vehicles, they outperform in terms of accuracy previous simulations found in the literature [7] [24]. Indeed, precision can be controlled in any integration method used when a functional description of the model is available instead of using the standard Braitenberg vehicle formulation.

Figure 5 presents the results of simulations performed for vehicle 2a under the stimulus function plotted on figure 5(a). The stimulus is the non-negative part of the product of three parabolic functions with positive and negative definite Hessian matrices, specifically $S(\mathbf{x}) = \prod_{i=1}^{3} S_i(\mathbf{x})$, where $S_i(\mathbf{x}) = g_i + \alpha_i(\mathbf{x} - \mathbf{x}_i^0)^T \Sigma_i (\mathbf{x} - \mathbf{x}_i^0)$ and the parameters for the functions are presented in table 3. The first function $S_1(\mathbf{x})$ implicitly defines the workspace as the region where $S_1(\mathbf{x}) > 0$ while the other two encode areas the vehicle should not traverse, where the functions take negative values. The product of the three functions will generate a positive stimulus inside the workspace, and the level set $S(\mathbf{x}) = 0$ is formed by the three ellipses with different orientations and sizes drawn in figures 5(b) and 5(c). The function $F(s)$ was chosen to be a linear function with positive slope going through the origin ($F(s) = 0.1s$). Figure 5(b) presents the trajectories obtained from simulating vehicle 2a with 60 different headings starting at position $\mathbf{x}^T = [0, 1]$. As expected, all the trajectories end at some point of the boundary ∂D where the stimulus takes a zero value, and the tangent to the trajectories at these points corresponds to the opposite direction of the gradient. The simulations for a starting point at $\mathbf{x}^T = [2, 5]$ for several heading directions are shown in figure 5(c) with a similar resulting behaviour. This kind of behaviour is useful, for instance,

i	g_i	α_i	Σ_i	$\mathbf{x}_i^0$
1	10	-0.1	$\begin{bmatrix} 1 & 0.2 \\ 0.7 & 3 \end{bmatrix}$	$[0, 0]$
2	-1	0.8	$\begin{bmatrix} 1.2 & 0 \\ 0 & 1 \end{bmatrix}$	$[-4, -3]$
3	-1	0.6	$\begin{bmatrix} 0.7 & 0.3 \\ 0.2 & 1 \end{bmatrix}$	$[-5, 0]$
4	-1	0.4	$\begin{bmatrix} 1 & 0.4 \\ -0.2 & 1.3 \end{bmatrix}$	$[-0.5, 3]$

Table 4: Parameters for the stimulus function $S(\mathbf{x})$ on the simulation of vehicle 2b

if we want a robot to leave a specific area or region of its environment. We therefore need to design a potential function that vanishes at the boundary of the area the robot has to abandon.

Figure 6(b) shows the simulated trajectory for Braitenberg vehicle 2b with a similar stimulus $S(\mathbf{x}) = \prod_{i=1}^{4} S_i(\mathbf{x})$, with the corresponding parameters shown in table 4. In this case there are three obstacle-like or forbidden areas inside the outer boundary of the workspace and the function $F(s) = m \tanh(\beta s)$ with $m = 1$ and $\beta = 5 \cdot 10^{-4}$. The hyperbolic tangent introduces saturation in the perceived stimulus and the maximum linear velocity is controlled through the parameter m. The resulting function composition $F(S(\mathbf{x}))$ is shown in figure 6(a), which can be seen as a linear velocity profile on the workspace. The level set where the stimulus takes zero value is also shown in figure 6(b) and it is the same set where the velocity of the vehicle vanishes since $F(0) = 0$. All the equilibria of the vehicle lay on ∂D and are unstable, but the velocity of the vehicle is not zero anywhere else. The resulting trajectory is presented in figure 6(b) and the simulation was stopped after 1000 simulated seconds. The instability of the boundary points can be observed in the trajectory, since when the vehicle approaches the boundary of positive stimulus it turns to come back to points of high stimulus value. Through simulations it can be seen that the trajectories of this vehicle display features of chaos, specifically, it displays sensitivity to initial conditions. This is just the consequence of the dynamical system having a unstable manifold everywhere in the state-space. Because of the transitivity property of chaotic systems, their trajectories are dense in the state space. This makes Braitenberg vehicle 2b suitable for

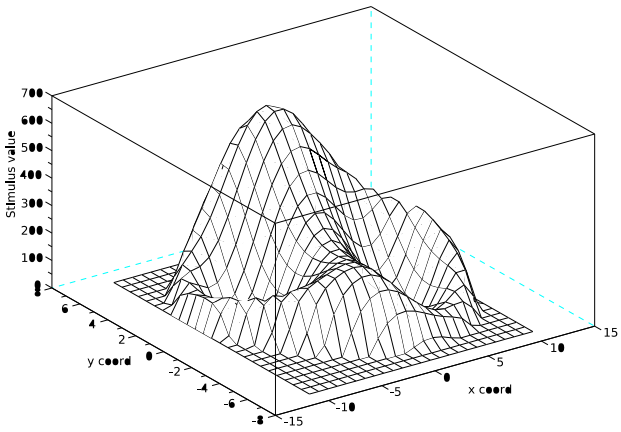

(a) Stimulus function $S(\mathbf{x})$ defined in a non-simply connected set.

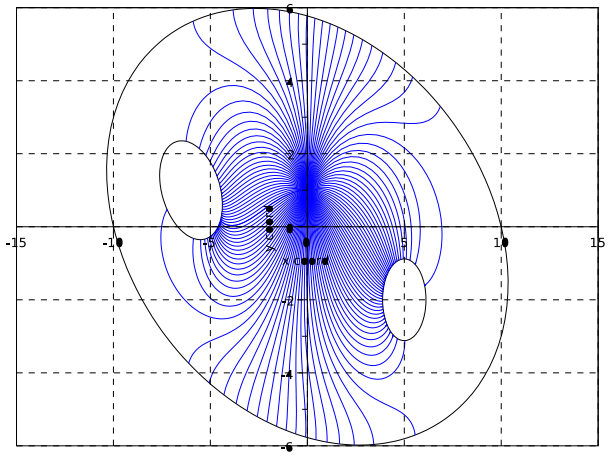

(b) Simulated trajectories starting at $(0, 1)$ with different heading directions.

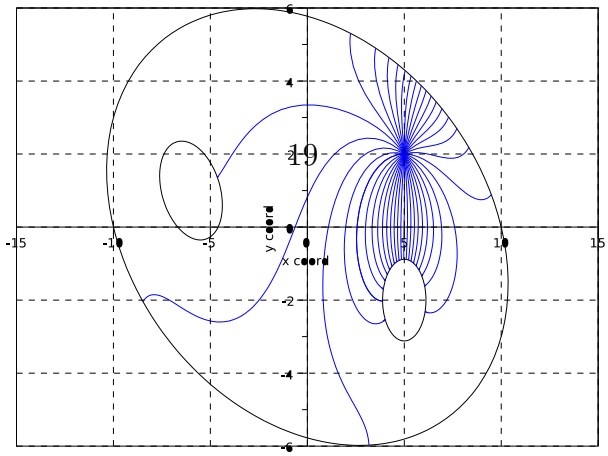

solving coverage problems in robotics.

Figure 7(b) shows 20 simulated trajectories of Braitenberg vehicle 3a with random initial conditions within the 2×2 square around the maximum of the stimulus function shown in figure 7(a). The initial heading of the vehicle was also chosen at random, and the selected functions for these trials are: $S(\mathbf{x}) = \frac{g_0}{1+\alpha \mathbf{x}^t \Sigma \mathbf{x}}$ and $F(s) = ms + b$, with $g_0 = 1$, $\alpha = 0.05$, $\Sigma = diag(1, 4)$, $m = -1$ and $b = 1$. In this case the workspace is $\Re^2$. Even though the motion of the vehicles continues, only the parts of the trajectories inside the 8×8 square around the stimulus are plotted. As it can be seen, all the trajectories move away from the stimulus maximum and there are preferred escaping direction almost all the simulated vehicles follow. This is a result of the stimulus not being circularly symmetric.

Figure 8 shows ten simulated trajectories starting from random poses of Braitenberg vehicle 3b using the same stimulus $S(\mathbf{x})$ (shown in figure 7(a)) and the same $F(s)$ as for vehicle 3a. The function $F(S(\mathbf{x}))$ vanishes at the maximum of the stimulus, which is the only equilibrium point in the workspace. Since the stimulus has no circular symmetry a preferred direction to reach the maximum and oscillatory behaviour appear in the trajectories. The simulations confirm that Braitenberg vehicle 3b can be used for target reaching.

5. Discussion and Further Work

This paper presents the first formal joint analysis of Braitenberg vehicles 2 and 3 modelled as systems of non linear differential equations. Even though their behaviour can be easily understood in an intuitive basis, applications for robotics require a formal methodology to select the stimulus or potential function and the internal wiring of the vehicle. In this paper we show that the expected behaviour of these vehicles, as intuitively understood, can be explained using the theoretical model and dynamical systems analysis. This model provides an easy and accurate way of simulating and understanding Braitenberg vehicles as a dynamical system, while previous works could not analyse the resulting trajectories from a theoretical standpoint [24] [7]. Furthermore, the model also helps identifying theoretically the conditions to properly design and implement Braitenberg vehicles, and provides theoretical support for the existing empirical works. Specifically, it can be found in the literature that Braitenberg vehicle 2b has been used to implement wandering mechanisms that incorporate obstacle avoidance, and vehicles 3a and

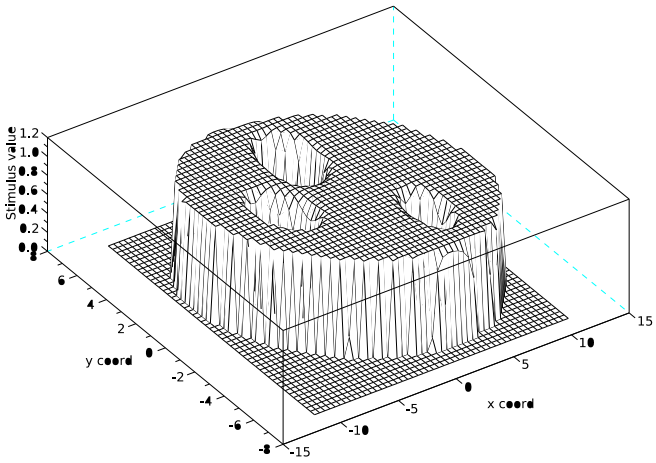

(a) Function composition $F(S(\mathbf{x}))$, defined in a non-simply connected set.

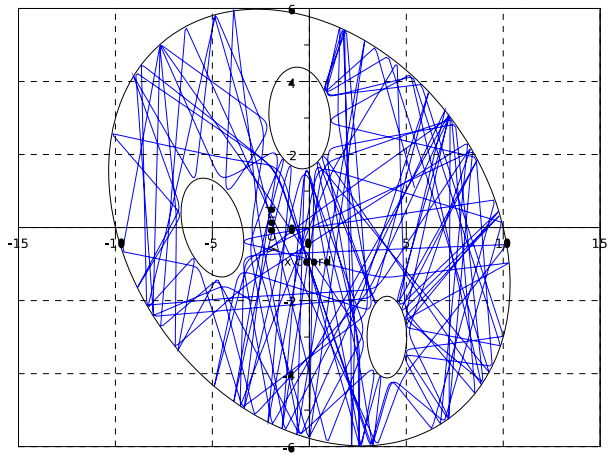

(b) One simulated trajectory that stays in D

Figure 6: Simulation of vehicle 2b

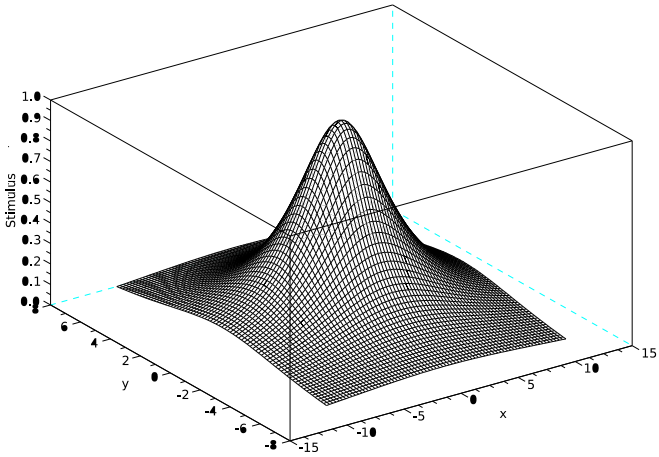

(a) Function composition $F(S(\mathbf{x}))$

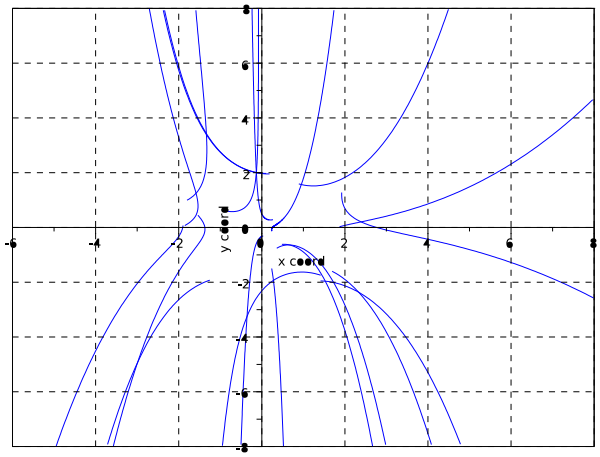

(b) Simulated trajectories

Figure 7: Simulations of vehicle 3a

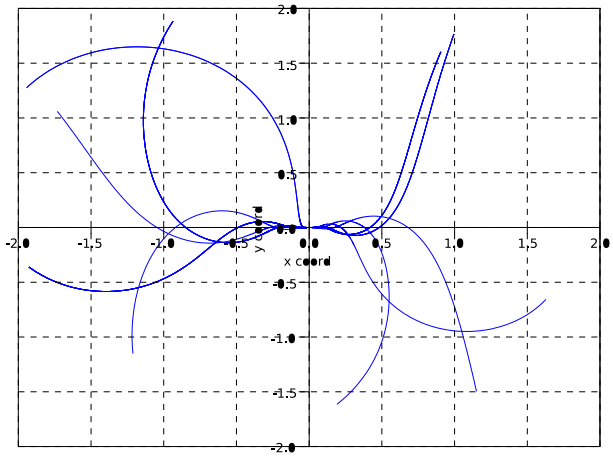

Figure 8: Ten simulated trajectories for the vehicle 3b starting with random poses

2a to implement goal seeking and avoidance behaviours respectively, when the appropriate stimuli are used. The present work backs up theoretically all these applications and paves the way for further robotic applications of Braitenberg vehicles in mobile robotics. To ensure the presented results apply, the right stimuli must be selected, and their mathematical properties have to be tested beforehand. An alternative would be to define an artificial potential function with the desired features such that the robot displays the expected behaviour. Examples of possible stimuli in mobile robotics include: the distance to some target or to the closest obstacle, light or sound intensity, the concentration of some gas in air, etcetera. Therefore, as we can also deduce from the literature review Braitenberg vehicles are widely applicable.

Real world applications of Braitenberg vehicles are mainly related to navigations tasks in robotics, since they implement what could be called navigation primitives. This paper deals with the simplest theoretical configuration, a single stimulus which generates different primitives depending on the vehicle used. On the other hand, normal environments have stimuli of different kinds, or multiple potential functions can be constructed, and therefore these primitives can be combined to implement more complex tasks. This will pro-

duce a richer behaviour and very complex equations that, probably, cannot be understood or analysed analytically. However, to deal with the more complex situations using the model presented on this paper, numerical methods can be used to accurately simulate the behaviour of the vehicle for specific stimulus settings. This is part of the evolution of Braitenberg vehicles, specifically vehicle 3c, although no specification is given [1] on how to solve the motor fusion problem, the combination of the primitives. Tasks like obstacle avoidance can be implemented using a combination of vehicles 2a (fear to obstacles, for instance) and 3a (taxis towards a target). The present paper develops on the grounds of the seminal work of Braitenberg, where noise is not accounted for. This might be a relevant issue if unstable manifolds exist in the state space, as the divergence will be likely increased by a stochastic component. For the stable case, however, intuition indicates that the effects of the noise will be kept within some bounds. Therefore, an important extension to this work is generating a model that will include the effect of noisy sensors, but this requires a different modelling approach, although the results presented here would correspond to average trajectories of a stochastic model.

A. Velocity equations of Braitenberg vehicles

Let us denote $\mathbf{x}_r$ and $\mathbf{x}_l$ the position of the right and left sensors of the vehicle, and $\mathbf{x}$ the midpoint between them. For any stimulus function $S(\mathbf{x})$ and function connecting the sensors to the motor wheels $F(s)$, we can write the velocities of the right and left wheels as:

$$v_r = F(S(\mathbf{x}_r)) \tag{11}$$
$$v_l = F(S(\mathbf{x}_l)) \tag{12}$$

for a-type or parallel vehicles, and

$$v_r = F(S(\mathbf{x}_l)) \tag{13}$$
$$v_l = F(S(\mathbf{x}_r)) \tag{14}$$

for b-type or crossed vehicles. Given the distance δ between the two sensors, and the coordinate frame linked to the front of the vehicle $\{\hat{e}, \hat{e}_p\}$, we can write the position of the left and right sensors as:

$$\mathbf{x}_r = \mathbf{x} - \frac{\delta}{2}\hat{e}_p \quad (15)$$

$$\mathbf{x}_l = \mathbf{x} + \frac{\delta}{2}\hat{e}_p \quad (16)$$

If we further assume both functions $S(\mathbf{x})$ and $F(s)$ are smooth (C^∞), we can approximate the velocities as Taylor series around the point $\mathbf{x}$ as:

$$\begin{aligned} F(S(\mathbf{x}_r)) &= F(S(\mathbf{x})) - \frac{\delta}{2}\nabla F(S(\mathbf{x}))^T\hat{e}_p \\ &+ \frac{\delta^2}{8}\hat{e}_p^T D^2F(S(\mathbf{x}))\hat{e}_p + O(\delta^3) \quad (17) \\ F(S(\mathbf{x}_l)) &= F(S(\mathbf{x})) + \frac{\delta}{2}\nabla F(S(\mathbf{x}))^T\hat{e}_p \\ &+ \frac{\delta^2}{8}\hat{e}_p^T D^2F(S(\mathbf{x}))\hat{e}_p + O(\delta^3) \quad (18) \end{aligned}$$

where $\nabla F(S(\mathbf{x}))$ is the gradient of $F(S(\mathbf{x}))$, $D^2F(S(\mathbf{x}))$ is the Hessian matrix and $O(\delta^3)$ are terms of at least order 3 on δ.

Given the wheelbase of the vehicle d, we can convert the wheel speeds, eqs. (11), (12), (13) and (14), to linear velocity ($v = \frac{v_r+v_l}{2}$) and turning rate ($\omega = \frac{v_r-v_l}{d}$) of the vehicles to get:

$$v = F(S(\mathbf{x})) + \frac{\delta^2}{2}\hat{e}_p^t D^2F(S(\mathbf{x}))\hat{e}_p + O(\delta^4) \quad (19)$$

$$\omega = \mp\frac{\delta}{d}\nabla F(S(\mathbf{x}))^t\hat{e}_p + O(\delta^3) \quad (20)$$

where the negative sign on equation (20) correspond to the a-type vehicles, and the positive to b-type.

References

[1] V. Braitenberg, Vehicles. Experiments in synthetic psycology, The MIT Press, 1984.

[2] G. Fraenkel, D. Gunn, The orientation of animals. Kineses, taxes and compass reactions, Dover publications, 1961.

[3] C. Buiu, Hybrid educational strategy for a laboratory course on cognitive robotics, IEEE Transactions on Education 51 (1) (2008) 100–107.

[4] R. Stolkin, R. Sheryll, L. Hotaling, Braitenbergian experiments with simple aquatic robots, 2007.

[5] C. Reynolds, Steering behaviors for autonomous characters, in: Proceedings of the 1999 Game Developers Conference, 1999, pp. 763–782.

[6] G. Arechavaleta, J. P. Laumond, H. Hicheur, A. Berthoz, An optimality principle governing human walking, IEEE Transactions on Robotics 24 (1) (2008) 5–14.

[7] M. Rosenkind, G. Winstanley, A. Blake, Adapting Bottom-up, Emergent Behaviour for Character-Based AI in Games, Springer, 2012.

[8] I. Rañó, A steering taxis model and the qualitative analysis of its trajectories, Adaptive Behavior 17 (3) (2009) 197–211.

[9] I. Rañó, The bio-inspired chaotic robot, in: Proceddings of the IEEE International Conference on Robotics and Automation, 2014, pp. 304–309.

[10] T. Salumäe, I. Rañó, O. Akanyeti, M. Kruusmaa, Against the flow: A braitenberg controller for a fish robot, in: Proceedings of the International Conference on Robotics and Automation (ICRA), 2012, pp. 4210–4215.

[11] A. J. Lilienthal, T. Duckett, Experimental analysis of gas-sensitive Braitenberg vehicles, Advanced Robotics 18 (8) (2004) 817–834.

[12] M. Bernard, S. N'Guyen, P. Pirim, B. Gas, J.-A. Meyer, Phonotaxis behavior in the artificial rat psikharpax, in: International Symposium on Robotics and Intelligent Sensors, IRIS2010, 2010.

[13] D. Shaikh, J. Hallam, J. Christensen-Dalsgaard, L. Zhang, A Braitenberg lizard: Continuous phonotaxis with a lizard ear model, in: Proceedings of the 3rd International Work-Conference on The Interplay Between Natural and Artificial Computation, 2009, pp. 439–448.

[14] B. Webb, A Spiking Neuron Controller for Robot Phonotaxis, The MIT/AAAI Press, 2001, pp. 3–20.

[15] A. Horchler, R. Reeve, B. Webb, R. Quinn, Robot phonotaxis in the wild: a biologically inspired approach to outdoor sound localization, Advanced Robotics 18 (8) (2004) 801–816.

[16] R. Reeve, B. Webb, A. Horchlerb, G. Indiveri, R. Quinn, New technologies for testing a model of cricket phonotaxis on an outdoor robot, Robotics and Autonomous Systems 51 (1) (2005) 41–54.

[17] V. Lebastard, F. Boyer, C. Chevallereau, N. Servagent, Underwater electro-naviagation in the dark, in: Proceedings of the International Conference on Robotics and Automation (ICRA), 2012, pp. 1155–1160.

[18] E. Bicho, G. Schöner, The dynamic approach to autonomous robotics demonstrated on a low-level vehicle platform, Robotics and Autonomous Systems 21 (1997) 23–35.

[19] I. Rañó, T. Smithers, Obstacle avoidance through Braitenberg's aggression behavior and motor fusion, in: Proc. of the 2nd European Conf. on Mobile Robots, 2005, pp. 98–103.

[20] X. Yang, R. V. Patel, M. Moallem, A Fuzzy-Braitenberg Navigation Strategy for Differential Drive Mobile Robots, Journal of Intelligent Robotic Systems 47 (2006) 101–124.

[21] L. Capozzo, G. Attolico, G. Cicirelli, Building low cost vehicles for simple reactive behaviors, in: Proceedings of the IEEE International Conference on Systems, Man, and Cybernetics, Vol. 6, 1999, pp. 675–680.

[22] L. Perko, Differential Equations and Dynamical Systems, Springer, 2006.

[23] R. Hilborn, Chaos and Nonlinear Dynamics: An Introduction for Scientists and Engineers, Oxford University Press, 2001.

[24] D. Terzopoulos, X. Tu, R. Grzeszczuk, Artificial fishes: Autonomous locomotion, perception, behaviour and learning in a simulated physical world, Artificial Life 1 (4).